Article:
Elbadawy, I, Gaskell, PH, Lawes, M et al. (1 more author) (2015) Numerical Investigation of the Effect of Ambient Turbulence on Pressure Swirl Spray Characteristics. International Journal of Multiphase Flow, 77. 271 - 284. ISSN 0301-9322

https://doi.org/10.1016/j.ijmultiphaseflow.2015.06.008

Numerical Investigation of the Effect of Ambient Turbulence on Pressure Swirl Spray Characteristics

Ibrahim Elbadawy[a,c*], Philip H. Gaskell[b], Malcolm Lawes[c] & Harvey M. Thompson[c,]

[a] Faculty of Engineering at El-Mattaria, University of Helwan, Masaken El-Helmia P.O., Cairo 11718, Egypt

[b] School of Engineering and Computing Sciences, University of Durham, Durham, DH1 3LE, UK

[c] Institute of Thermofluids, School of Mechanical Engineering, University of Leeds, Leeds, LS2 9JT, U.K.

Abstract

A numerical investigation is performed into the effects of the root mean square (RMS) turbulence velocity on the spray characteristics of liquid fuel injected into a constant volume vessel and comparison drawn with experimental data obtained for the case of iso-octane fuel injected into nitrogen showing good agreement between the two. A detailed parametric study is undertaken, enabling the effect of ambient turbulence on key spray characteristics to be determined. The numerical solutions obtained reveal how an increased level of turbulence in the gas into which fuel is injected leads to reductions in the axial fuel penetration and the Sauter mean droplet diameter, together with increases in radial vapour penetration and the number of fuel droplets formed.

Keywords: Fuel injection; Spray characteristics; Experiments, Computational Fluid Dynamics

1. Introduction

Liquid sprays have a diverse range of applications that include agriculture, combustion, medicine, the cosmetics industry and separation technologies, where different injector technologies are adopted to produce a desired overall spray structure and droplet size distribution (Bafekr et al., 2011). In particular, spray atomisation within the fuel systems of spark ignition (SI) engines has received considerable attention over the last two decades, such that traditional carburetion has now been almost universally superseded by fuel injection. Port Fuel Injection (PFI) inserts fuel into the intake port of

each cylinder to, for example, improve Specific Fuel Consumption (SFC). An important issue with the latter is that it may lead to significantly increased UnBurned HydroCarbon (UBHC) emissions due to partial burn in the first 4-10 cycles following a cold start (Zhao et al., 1999). This has led to increased interest in an alternative approach, that of Gasoline Direct Injection (GDI). Here, significantly higher injection pressures lead to much better atomisation and mixing, which are particularly important during cold start conditions. Takagi (1998), for example, found that cold start UBHC emissions and fuel consumption from a Nissan prototype GDI engine were respectively 30% and 20% lower than those from a comparable PFI engine. Other advantages of GDI include its ability to run in stratified charge mode, with improved combustion stability and significantly reduced throttling losses (Zhao et al., 1999).

The improved design and subsequent performance of GDI engines requires a sound understanding of the associated fluid flow mechanisms and the parameters which influence them. Of key importance is the fuel atomisation process which increases the fuel surface area and improves the efficiency of fuel evaporation and combustion within engines. A number of previous experimental studies have demonstrated that spray characteristics, such as spray penetration length, cone angle and droplet sizes and their distribution are mainly affected by: (i) the internal geometry of the injector and the nozzle geometry such as diameter and length, (ii) fuel properties, (iii) the properties of the ambient gas into which the spray is injected and (iv) the differences between the injection and ambient pressures (Gao et al., 2005; Pastor et al., 2008; Elbadawy et al., 2011).

The nozzle diameter has a significant effect on the penetration length. It has been found that a decrease in nozzle diameter leads to a shorter penetration length due to an earlier onset of secondary breakup (Martínez et al., 2008). Moreover, Lucchini et al., (2010) showed the steady liquid penetration length to increase linearly with increasing orifice diameter. Cooper and Yule (2001) studied the effect of nozzle length on the spray characteristics using a high pressure swirl atomiser. It was found that increasing the nozzle length leads to a reduced ratio of radial momentum to axial momentum and therefore to a reduced cone angle.

Experimental studies have also revealed fuel surface tension and viscosity to have a significant influence on spray atomisation. The former resists the formation of smaller droplets, with the Weber number having the greatest influence on droplet size distribution (Agudelo et al., 2009). In general, higher fuel viscosity impedes spray atomisation, where the increased friction results in a coarser, narrower spray that can collapse into a straight fuel stream at very high viscosities. The effect of injection and ambient pressures on the atomisation process has similarly been investigated widely. It has been shown how larger injection pressures produce smaller droplets and larger spray penetration lengths (Pastor et al., 2008; Ryu et al., 2005), whereas the increased resistance to flow from larger ambient pressures results in a reduced spray penetration length and increased spray cone angles (Gao et al., 2005).

The increasing power and accuracy of numerical methods for solving the governing associated equations of motion have resulted in several recent Computational Fluid Dynamics (CFD) investigations of fuel atomisation in quiescent ambient gases, with the individual influences of the injection and ambient pressures on the atomisation process being the focus of studies. Many studies have used the Discrete Phase Modelling (DPM) approach where simulations of the turbulent gas phase have been coupled with a variety of models for liquid evaporation, breakup and drag. The turbulent gas phase simulations can be carried out using either Large Eddy Simulations (see e.g. Jiang et al., 2010 and Banaeizadeh et al., 2013) or more commonly using a sequence of RANS simulations at a series of time-steps. The computational studies indicated below are a selection of studies which have used successfully some form of coupled DPM/RANS approach for the liquid and gaseous phases, respectively. Beck and Watkins (2004) and Bafekr et al. (2011), for example, investigated the effect of injection pressure on important spray characteristics, such as spray cone angle, penetration length and width, evaporation rate and Sauter mean droplet diameter, D_{32}. Their main findings were that injection pressure has little effect on spray cone angle but has a significant effect on the spray penetration length. Beck and Watkins (2004) and Lim et al. (2004) also showed how increasing the ambient pressure of the quiescent gas into which the fuel is injected leads to a reduced spray penetration length and reduced Sauter mean droplet diameter.

Both of the above findings are physically reasonable due to the increased aerodynamic resistance offered by quiescent gas of higher pressure. The more recent computational work of Desantes et al. (2009), into the effect of quiescent gas density on spray characteristics, is consistent with these earlier findings, but also shows that spray cone angle increases as the gas density is increased.

All of the above have considered spray atomisation for the idealised case of fuel injected into a quiescent gas. However this situation is rarely achieved in practice since in most applications, such as the in-cylinder flow of internal combustion (IC) engines, the flow is highly turbulent. In IC engines, the turbulence is uncontrolled due to the changes of the RMS turbulent and mean velocities with the engine speed and throttle opening, (Burluka et al., 2012); many experimental and computational investigations have appeared which study the spray and combustion characteristics in real engine conditions. Recent examples of the former include the work of Kim et al. (2013), who compared the spray characteristics for gasoline and diesel fuel under non-evaporating (in a constant volume chamber) and evaporating (in an engine) conditions, and studies on the effect of injection timing on one stage (Oh and Bae, 2013) and two stage (Turkcan et al., 2014) direct injection strategies. CFD has also been widely used to study injection processes in IC engines. Wei et al. (2014), for example, used CFD to explore the effect of nozzle angle on the spray characteristics, mixture formation and emissions, while Su et al. (2014) considered the effect of combustion chamber geometry on the fuel/air mixture and equivalence ratio.

The complex, time-dependent nature of real engine flows increases the difficulty of understanding the effects of the ambient flow conditions, in the gas into which the fuel is injected, on the resultant spray atomisation. Radwan et al. (2014)'s computations, for instance, reported that the RMS turbulent velocity is very sensitive to piston location and, as a result, during the injection process the spray is influenced strongly by the varying turbulence level. Attempts have therefore been made to generate controlled turbulent flow in the ambient gas. One approach is to use grids placed in front of an injector, but these result in heterogeneous turbulence with spatially varying turbulence levels and integral length scales. This has been employed by Takeuchi and Douhara (2005, 2008) to demonstrate that turbulence intensity has a strong influence on the dispersion and evaporation of droplets. In

contrast, Jakubik et al. (2006) used a fan-stirred closed vessel to generate nearly isotropic turbulence levels in order to carry out a brief study of its effect on diesel spray penetration length and spray angle. An alternative approach to studying the effect of controlled turbulence levels on spray penetration length and width, and the interactions between the liquid and vapour phases, is to do so computationally. The work presented here is the first to use such an approach to investigate the influence of controlled ambient turbulence on the liquid fuel injection and spray formation processes.

The paper is organised as follows. Section 2 describes the problem under investigation and includes a brief discussion of the experimental methodology used to generate the data for comparison purposes. Section 3 provides an overview of the mathematical modelling of the fuel atomisation process and method of solution while Section 4 describes the comprehensive series of results obtained. Conclusions are drawn in Section 5.

2. Problem Specification

The problem of interest is that of fuel injection into well defined steady, near homogeneous and isotropic ambient flow field at pressures, temperatures and turbulence levels of relevance to engine investigations (Elbadawy et al., 2011). The geometry of interest, shown in Fig. 1(a), has an internal diameter of 380 mm and a central, spherical focussing volume of 150 mm diameter. The injection process was visualised through three orthogonal 100 mm thick and 150 mm diameter quartz windows. Four fans driven by 8 kW variable speed motors were positioned near the internal vessel wall generating isotropic turbulence in the central volume, with a linear relationship between the fan speed and RMS turbulence velocity. Previous studies have shown that the turbulence integral length scale in the central volume is effectively independent of fan speed and equal to 20 mm (Nwagwe et al., 2000). For the experimental component of the work, the fan speed was adjusted to yield the desired RMS turbulence velocity in the central volume into which the fuel is injected. The pumping unit shown in Fig. 1(b) pumped fuel under high pressure to the injector and was comprised of a 12 V low pressure (LP) pumping circuit which fed the second, high pressure, pumping circuit (HP) through a fuel filter. The LP pump ensured that the fuel pressure was above 2 bar to prevent cavitation in the HP pump. The latter was driven by a three phase variable speed motor which adjusted the injection pressure up

to a maximum 120 bar. A handle throttle valve manually regulated the injection pressure and ensured that the liquid fuel emerged from the injector into the gas at the required conditions; a high pressure swirl fuel injector (Volkswagen AG), that is commonly found in modern GDI engines, was employed for this purpose.

Figure 1(c) is a schematic showing the imaging techniques employed which provided simultaneous visualizations of the vapour and liquid phases. The liquid phase was visualized using a Mie-scatter laser sheet, while the vapour phase captured using the Schlieren imaging; these were recorded by a high speed digital camera. Further details of the experimental methods and equipment used to generate the experimental data can be found in Elbadawy et al. (2011).

3. Mathematical Model

The above fuel injection problem is solved within the enclosed spherical flow domain illustrated in Fig. 2(a). The turbulence generated by the fans is modelled by flow through eight cylindrical inlets, each of which has two boundaries as shown in Fig. 2(a): an inlet one where the inflow velocity is prescribed and the gas flows radially outwards and an outlet one, where the gas leaves the cylinder in a tangential direction. The injection region of interest, shown in Fig. 2(b), is formed by a cube with 140 mm sides and the turbulence level within it varied by specifying the value of the inlet velocity at the cylindrical boundaries. The cube is meshed uniformly in order to avoid inaccuracies that have been shown to arise when non-uniform grids are used in the injection region (Lucchini et al., 2010).

3.1 Governing Flow Equations

During atomisation the liquid fuel evaporates and fuel vapour mixes with the ambient gas with the result that the coupled gas (continuous) and liquid fuel (discrete) phases must be modelled simultaneously. Flow within the gas phase is modelled by the Navier-Stokes and continuity equations, namely:

$$\frac{\partial}{\partial t}(\rho \underline{u}) + \nabla.(\rho \underline{u}\underline{u}) = -\nabla p + \nabla.\underline{\underline{\tau}} + \rho \underline{g}, \qquad (1)$$

$$\frac{\partial \rho}{\partial t} + \nabla.(\rho \underline{u}) = 0\,, \tag{2}$$

where ρ is the density of the gas (a mixture of the ambient gas and fuel vapour), p is the pressure, $\underline{u}$=(u,v,w) is the instantaneous gas velocity, $\underline{g}$ is the acceleration due to gravity and

$$\underline{\underline{\tau}} = \mu \left[\nabla \underline{u} + (\nabla \underline{u})^{T} - \frac{2}{3} \nabla.\underline{u}\ \underline{\underline{I}} \right] \tag{3}$$

is the Newtonian stress tensor, where μ is the gas viscosity and $\underline{\underline{I}}$ is the unit tensor. The presence and motion of liquid within the gaseous phase increases the momentum exchange between the two phases and the right hand side of the momentum equation (1) is supplemented by an additional term, $\rho \underline{F}^{s}$, which represents the momentum gained by the gas phase due to the spray, Wright (2005).

In practical fuel injection systems, turbulence plays an important role in enhancing fuel mixing and evaporation. In the present study the effects of turbulence are modelled using popular Reynolds Averaged Navier-Stokes (RANS) approaches that have been used successfully in previous related work. One of these is the k-ε model, see e.g. Nishida et al. (2009), which is based on two extra transport equations for the turbulent kinetic energy, k, and the turbulent dissipation rate, ε, which take the form:

$$\frac{\partial}{\partial t}(\rho k) + \nabla(\rho k \underline{u}) = \nabla.\left[\left(\mu + \frac{\mu_t}{\sigma_k} \right) \nabla k \right] + G_k + G_b - \rho\varepsilon - Y_M + S_k\,, \tag{4}$$

$$\frac{\partial}{\partial t}(\rho \varepsilon) + \nabla(\rho \varepsilon \underline{u}) = \nabla.\left[\left(\mu + \frac{\mu_t}{\sigma_\varepsilon} \right) \nabla \varepsilon \right] + C_{1\varepsilon} \frac{\varepsilon}{k} \left(G_k + C_{3\varepsilon} G_b \right) - C_{2\varepsilon} \rho \frac{\varepsilon^2}{k} + S_\varepsilon \tag{5}$$

respectively. The term G_b is given in terms of buoyancy and temperature gradient, via

$$G_b = \beta . \underline{g} \frac{\mu_t}{Pr_t} \frac{\partial T}{\partial x_i}, \tag{6}$$

where Pr_t is the turbulent Prandtl number for energy and $\underline{g}$ is the gravitational vector. The coefficient of thermal expansion, β, is defined by

$$\beta = -\frac{1}{\rho}\left(\frac{\partial \rho}{\partial T}\right)_p \quad , \tag{7}$$

while the G_k term represents the reduction in turbulent kinetic energy and is given by

$$G_k = -\rho\overline{u_i' u_j'}\frac{\partial u_j}{\partial x_i} \quad . \tag{8}$$

Y_M represents the contribution of the fluctuating dilatation in compressible turbulence to the turbulent dissipation rate due to high Mach number and is given by

$$Y_M = 2\rho\varepsilon M_t^2 \quad , \tag{9}$$

where M_t is the turbulent Mach number $\left(M_t = \sqrt{\frac{k}{a^2}}\right)$ and a is the speed of sound.

The parameters σ_k = 1.0 and σ_ε =1.3 represent the turbulent Prandtl numbers for k and ε, respectively and S_k and S_ε are user defined source terms. The other parameters take the recommended default values $C_{1\varepsilon}$=1.44, $C_{2\varepsilon}$=1.92 and $C_{3\varepsilon}$=0.09, see e.g. Boulet et al. (2010). Also considered here are the RNG k-ε model (Bafekr et al., 2011) and the Reynolds Stress model, the latter being the most general and computationally expensive model which solves six additional transport equations for each of the Reynolds stress components.

3.2 Species and Energy Transport Equations

The gas phase is composed of two species, namely the ambient gas and fuel vapour. The density of each phase within the gas is represented by $\rho_i = \rho\ Y_i$, where ρ is the density of the ambient gas/fuel vapour mixture and Y_i is the mass fraction of species i (i=1 for the gas and i=2 for the fuel vapour). The equation for fuel vapour transport within the gaseous phase takes the form

$$\frac{\partial}{\partial t}(\rho_2) + \nabla.(\rho_2 \underline{u}) = -\nabla.\underline{J_2} + R_2 + S_2 \tag{10}$$

,

where R_2 is the rate of production of the fuel vapour and S_2 is the rate of its creation from the dispersed phase plus any user defined sources. The diffusion flux in equation (10) is given by

$$\underline{J}_2 = -(\rho D)\nabla Y_2, \tag{11}$$

in terms of the diffusion coefficient of the fuel vapour species in the ambient gas, D.

Energy conservation within the gaseous phase is represented by the following energy equation

$$\frac{\partial}{\partial t}(\rho h) + \nabla.(\rho h \underline{u}) = \nabla.\left[\lambda \nabla T + \rho D \sum_{i=1}^{N} h_i \nabla Y_i\right] + \rho\varepsilon \ , \tag{12}$$

where h is the enthalpy of the ambient gas/fuel vapour mixture, λ is the thermal conductivity of the ambient gas and h_i is the specific enthalpy of species i. The second term in the square brackets of Eq. (12) describes the energy transfer associated with mass diffusion of species i in the liquid/gaseous phase flow and the last term on the right hand side is the dissipation of turbulent kinetic energy, which is used in the Discrete Phase Model (DPM) outlined below.

3.3 Spray Modelling

Spray flows are complex multi-phase flows in which the droplet motions are stochastic and influenced by droplet breakup and coalescence in addition to hydrodynamic drag and gravitational forces. Here, the DPM is used to model the injection of non-reacting iso-octane into ambient nitrogen, via a stochastic tracking model for the dispersion of the fuel droplets (Bafekr et al., 2011; Fangwei et al., 2014). Drag forces between iso-octane droplets and surrounding nitrogen are modelled using the Dynamic Drag Model (DDM) (Jiang et al., 2010) where the drag coefficient is calculated first under the assumption that the droplets are spherical, before being corrected as follows

$$C_{d,Sphere} = \begin{cases} \frac{24}{Re}\left(1 + \frac{1}{6}Re^{\frac{2}{3}}\right) & Re \leq 1000, \\ 0.424 & Re > 1000, \end{cases} \tag{13}$$

where the applicable regime is governed by the droplet Reynolds number, $Re = \frac{\rho u_{rd}\, d}{\mu}$, in which d is the droplet diameter, u_{rd} is the relative velocity between the droplet and ambient gas, and ρ and μ are the ambient gas density and molecular viscosity, respectively.

The spherical shape assumption is not entirely satisfactory due to droplet distortion caused by large droplet Weber number (ratio of inertial to surface tension forces), and the droplet diameters and high

relative velocity. In the DDM, a linear relation between a $C_{d,Sphere}$ and one of distorted shape is assumed by

$$C_d = C_{d,sphere}(1 + 2.632\Phi), \tag{14}$$

where Φ is the droplet distortion parameter, calculated from the second order ordinary differential equation

$$\frac{d^2\Phi}{dt^2} = \frac{C_F}{C_b}\frac{\rho_g}{\rho_L}\frac{u_{rd}^2}{r^2} - \frac{C_S\sigma}{\rho_L r^3}\Phi - \frac{C_D\mu_L}{\rho_L r^2}\frac{d\Phi}{dt}, \tag{15}$$

This calculation of the droplet distortion is based on an analogy with an equivalent spring-mass system where the first term on the right hand side of equation (15) represents the external drag force, the second term a spring constant due to surface tension and the third term, a damping parameter due to viscosity. The adjustable dimensionless constants have been determined by comparing theoretical results with experimental data and the following values suggested: $C_S = 8$, $C_D = 5$, $C_b = 0.5$ and $C_F = 1/3$ (Schmidt et al., 1999). However, Grover et al. (2002) have reported that a value of $C_S = 6$ is more appropriate in direct gasoline applications. Φ lies between the limits of a sphere $\Phi = 0$ and flattened droplet or disk $\Phi = 1$ that has drag coefficient $C_d = 1.54$ (Jiang et al., 2010).

Due to the impracticality of explicitly tracking the interactions between all fuel droplets during spray atomization, the DPM model significantly reduces the computational cost by modelling liquid interactions as those between a series of discrete liquid parcels, each of which contains a large number of droplets with similar properties and which do not interact with each other (Jiang et al., 2010). When fuel exits the injector, a liquid jet atomises into small droplets due to mass, momentum and energy exchange between the fuel and ambient gas. In the region near the nozzle exit, in which the Weber number is large, thin liquid ligaments form at the liquid-gas interface due to instability, termed primary breakup. Subsequently, these ligaments fragment to form small droplets, the secondary breakup phase. The primary breakup can be modelled using a Volume-of-Fluid (VOF) algorithm coupled to a Lagrangian particle tracking model to simulate the motion and the influence of the smallest droplet (Tomar et al., 2010). Following Bafekr et al. (2011) and Fangwei et al. (2014) the

Linearized Instability Sheet Atomisation (LISA) model is used to simulate the atomisation process of a pressure swirl nozzle.

The secondary breakup model depends mainly on the droplets generated following primary breakup. According to the experimental observations of Faeth et al. (1995), there are three secondary breakup regimes: bag, shear/stripping and catastrophic breakup. These regimes depend only on the Weber number of the droplet (Bafekr et al., 2011), which is given by:

$$W_e = \frac{\rho_g u_{rd}^2 d_0}{\sigma}, \tag{16}$$

where ρ_g and σ are the gas density and droplet surface tension respectively and d_0 is the initial droplet diameter estimated by the LISA model. The Weber number is also used to distinguish between different breakup models according to its value (Bafekr et al., 2011). For instance, if We <100 then the Taylor Analogy Breakup (TAB) model is employed, while the surface wave instability (WAVE) model is used for We >100, Rotondi and Bella (2006).

Note that since the Weber number at the nozzle exit being considered is typically greater than 100, secondary droplet breakup is modelled using the WAVE model where aerodynamic forces and the relative velocity between the liquid and gas phases cause fluctuations and waves which are responsible for the spray atomisation. Both continuity and momentum equations are utilised to describe these fluctuations leading to the following dispersion equations for the wavelength (Λ) and wave growth rate (Ω):

$$\frac{\Lambda}{a} = 9.02 \frac{(1+0.45Oh^{0.5})(1+0.4Ta^{0.7})}{(1+0.87\,We_g^{1.67})^{0.6}}, \tag{17}$$

$$\Omega \left[\frac{\rho_L a^3}{\sigma}\right]^{0.5} = \frac{0.34 + 0.38We_g^{1.5}}{(1+Oh)(1+1.4Ta^{0.6})}, \tag{18}$$

where $Oh = \sqrt{We_L}/Re_L$ is the Ohnesorge number and $Ta = Oh\sqrt{We_g}$ is the Taylor number. Furthermore, $We_L = \rho_L u_{rd}^2 a/\sigma$ and $We_g = \rho_g u_{rd}^2 a/\sigma$ are the Weber numbers for the liquid and gas, respectively; $Re_L = u_{rd} a/\upsilon_L$ is the Reynolds number and 'a' is the characteristic radius of blobs (large drops) (Jiang et al., 2010).

Understanding the evaporation of the discrete phase is very important to the spray atomisation process. Moreover, the fuel evaporation rate has a big influence on the burning velocity and combustion efficiency (Sulaiman, 2006; Saat, 2010). The evaporation rate of the droplet vapour into the ambient gas depends mainly on the vapour concentration between the droplet surface and the bulk gas. Accordingly, the mass flux of the droplet vapour into the gas is calculated via

$$N_i = h_{cm}\left(C_{i,s} - C_{i,\infty}\right), \tag{19}$$

where N_i is the molar flux of the vapour, $C_{i,s}$ and $C_{i,\infty}$ are the vapour concentration at the droplet surface and in the bulk gas, respectively, and h_{cm} is the convective mass transfer coefficient.

These parameters are given by

$$C_{i,s} = \frac{P_{sat}(T_d)}{RT_d}, \tag{20}$$

$$C_{i,\infty} = X_i \frac{P_\infty}{RT_\infty}, \tag{21}$$

where P_{sat} is the saturated pressure of the liquid at droplet temperature T_d and R is the universal gas constant; X_i is the bulk mole fraction of species i, and P_∞ and T_∞ are the ambient bulk gas pressure and temperature, respectively.

Finally, the convective mass transfer coefficient can be calculated from the Sherwood number, Sh, (Ashgriz, 2011), namely:

$$Sh = \frac{h_{cm}d}{D} = 2.0 + 0.6Re_d^{1/2}Sc^{1/3}, \tag{22}$$

where D is diffusion coefficient of the vapour in the bulk gas, Sc is the Schmidt number, $\frac{\mu}{\rho D}$, and d is the droplet diameter. The evaporated liquid flux is then calculated from Eq. (19) so that the new droplet mass can be calculated from:

$$m_d(t + \Delta t) = m_d(t) - N_i A_d M_{w,i} \Delta t, \tag{23}$$

where m_d is the droplet's mass, $M_{w,i}$ is the species molecular weight, and A_d is the droplet surface area.

Due to the difference in temperature between T_d and the ambient bulk gas temperature T_∞ there is heat transfer between the droplet and ambient gas. As a result the temperature of the droplet changes and this is calculated by applying a heat balance:

$$m_d C_p \frac{dT_d}{dt} = h_c A_d (T_\infty - T_d) + \frac{dm_d}{dt} h_{fg} \ , \quad (24)$$

where C_p is the droplet heat capacity, h_{fg} is the latent heat, and h_c is the convective heat transfer coefficient that is calculated from the Nusselt number, Nu (Ashgriz, 2011), by:

$$Nu = \frac{h_c d}{k_\infty} = 2.0 + 0.6 Re_d^{1/2} Pr^{1/3} \ . \quad (25)$$

where k_∞ is the gas phase thermal conductivity, and Pr is the Prandtl number of the gas phase, $\left(C_p \mu / k_\infty\right)$. The droplet temperature T_d is then calculated and updated via Eq. (24).

Further details on the DPM modelling approach employed can be found in Fangwei et al., (2014). Equations (1) to (25) are solved numerically using ANSYS (FLUENT). The typical flow conditions in the experimental and computational investigations are summarised in Table 1.

Parameter	Experimental/Modelling
Ambient gas	Nitrogen
Ambient Temperature [K]	300
Ambient density [kg.m^{-3}]	1.14
Ambient turbulence levels, ú [m.s^{-1}]	0, 1, 2, 4
Fuel	iso-octane
Fuel Density [kg.m^{-3}]	691
Fuel Viscosity [kg.m^{-1}.s^{-1}]	0.00054
Fuel surface tension [kg.s^{-2}]	0.021
Fuel diffusivity [m^{2}s^{-1}]	5.05 x 10^{-6}
Fuel temperature [K]	298
Injector type	pressure swirl atomizer
Hole diameter [µm]	570
Injection pressure [bar]	120
Injection duration [ms]	4.5
Calculation period [ms]	6.0

Table 1: Flow conditions considered.

4. Results and Discussion:

The experimental data provides boundary conditions for the CFD analyses, including the spray half cone angle θ^o at different RMS turbulence velocities, for the DPM spray model, and fuel mass flow rate [$\dot{m}_{\text{fuel}}$] as indicated in Table 2. A series of results is presented which investigate the effect of ambient turbulence level on vapour penetration length and width, fuel vapour mass fraction, flow field characteristics, and droplet density and diameter distribution, as the fuel spray atomisation proceeds. Due to the stochastic nature of the spray formation process, the CFD results presented are based on

the average of three CFD simulations, however in practice it is found that the variation in the predictions from the CFD simulations is quite small (typically between 2.5-4%)

P_{inj} [bar]	u' [m/s]	θ^o	$\dot{m}_{fuel}$ [g/s]
120	0	24^o	11.8
	1	28^o	
	2	31^o	
	4	33^o	

Table 2: Inlet conditions used in the DPM model.

The influence of mesh density is investigated first for the case of injection into quiescent and turbulent ambient nitrogen with u'=0 and 4 m/s, respectively. Following e.g. Nishida et al. (2009), turbulence is modelled using the standard k-ε model. Vapour penetration length, S_V, and vapour penetration width, W_V, are key spray atomisation parameters; Fig. 3 shows the effect of mesh density, in the injection region, on the prediction of these quantities for mesh refinements based on the grid ratio (GR) which equals the ratio of grid length, L, to injector diameter, D_j. Following Lucchini et al. (2010), solutions are obtained with GR=17, 8 and 4 and a time-step Δt=0.1 ms. Note that the results are found to be insensitive to the particular choice of time step and Δt=0.1 ms is used in all the simulations presented below.

Figure 3 shows that predictions of S_V and W_V with GR=8 and GR=4 are in good agreement (typically 2-3% difference) and are in reasonable agreement with experiment. The poorer agreement of the predicted values of S_V with experiment at later times is due to modelling the laminar, quiescent gas flow using a turbulence model. Better agreement with the experimental data is achieved if the laminar flow model is used instead of a turbulence model, as indicated in Fig. 3(a) for GR=8. In addition, the CFD results for injection into a turbulent ambient gas using the turbulence model are generally in much better agreement with experiment as discussed below. Figure 4 shows the effect of GR on the fuel vapour mass fraction along the injector axis, f_{cl}, and with radial distance, f, at a plane 30 mm from the injector exit at t=4 ms after the start of injection. The shapes of the curves for the two finest grids are consistent and the use of a finer grid leads to slightly greater fuel transport in the axial direction.

Along the injector axis, the finer grid leads to a slightly (9%) larger peak near the injector and a slightly (4%) reduced downstream peak, whereas in the radial direction, the reduced radial transport of fuel is demonstrated by the upstream shift in the fuel vapour mass fraction curve. Figure 5 shows the effect of GR on the Sauter mean droplet diameter, $D_{32,}$ and number of droplets, N. As found by Lucchini et al. (2010), the influence of GR is small with the peak number of droplets for GR=4 being approximately 7% larger than for GR=8, while the variation in Sauter mean droplet diameter is even smaller. On the basis of these findings, all results reported subsequently have been obtained using a grid with GR=8 in the injection region, as a suitable compromise between computational requirements and solution accuracy.

The influence of the choice of RANS turbulence model is considered next. Figure 6 compares predictions of the effect of the ambient turbulence on S_V and W_V using the standard k-ε, RNG k-ε and Reynolds Stress RANS turbulence models with the experimental data of Elbadawy et al (2011). All three turbulence models' predictions are found to be in reasonable agreement with the experimental data and that the agreement generally improves at higher turbulence. Overall, the standard k-ε model provides the closest agreement with the experimental results, and shows quantitatively how the higher turbulence restricts the penetration of fuel in the axial direction and promotes spray penetration in the radial direction. The effect of the choice of turbulence model on D_{32} and N is shown in Fig. 7. At the later times, the standard k-ε model's predictions lie between those of the other two models and after 6ms the maximum discrepancies between the k-ε models are approximately 7% and 13% for D_{32} and N, respectively. The standard k-ε model was used to produce all subsequent results.

The experimental results have been obtained in a fan-stirred vessel that generates nearly isotropic turbulence in the fuel injection region. Figure 8 shows that the CFD model produces approximately uniform turbulence, shown as contours of the RMS turbulence velocity, in the fuel injection region for cases with u' equal to 1 m/s, 2 m/s and 4 m/s. The predicted contours agree well with corresponding experimental data provided in Figs. 6.11-6.13 of Gunnar (2008).

Figure 9 compares experimentally obtained images of fuel liquid and vapour distribution with predicted images of fuel vapour mass fraction at t=4 ms and t=6 ms after the start of injection. As

discussed above, the experimental images were obtained from Mie scatter laser sheet and Schlieren techniques for two ambient conditions, u'=0 m/s and u'=4 m/s. The results are in generally good agreement in terms of spray size and shape. Figures 10 (a, b and c) more clearly reveal the effect of ambient u' on fuel evaporation into the ambient gas. Figures 10 (a) and (b) show the predicted effect of u' on the fuel vapour mass fraction along the axis of the injector, f_{cl}, at t=4ms and t=6ms, respectively. All the profiles are similar in shape and show clearly how an increased ambient u' increases the fuel's evaporation and restricts the penetration of fuel into the ambient gas in the axial direction. Figure 10(c) shows corresponding mass fraction data in the radial direction, f, at a plane normal to spray flow direction and 60 mm apart from the injector; in this case, the increased fuel penetration in the radial direction leads to increased fuel vapour mass fractions in the radial direction. For example, the area under the curve when u'=4 m/s is approximately 90% larger than for the laminar case.

Figure 11 shows the effect of ambient turbulence on the resultant flow field in greater detail. For the quiescent case (u'=0 m/s) the shear stresses generated around the surface of the spray lead to the formation of a primary vortex around the side of the spray, which moves in the axial direction with the main fuel jet. This vortex plays an important role in entraining gas into the fuel spray, leading to eventual evaporation of the fuel. For u'=4 m/s, the increased shear stresses cause the fuel jet to spread radially with a resultant reduction in axial penetration. In this case the stronger primary vortex leads to improved gas-fuel mixing, increasing the fuel's evaporation rate. Figures 12 and 13 show the effect of ambient turbulence on the axial velocity in the axial, V_{ac}, and radial, V_{ar}, directions. As seen from earlier results, Fig. 11, V_{ac} decreases as u' increases due to increased aerodynamic resistance which also results in more rapid radial spreading of the fuel jet. Figure 13 provides further information about the axial velocity in the radial direction along a line normal to the injector axis and 60 mm apart from the injector exit at t=4 and 6 ms. At both times, the velocity near the centre line reduces rapidly with radial distance, particularly for the low RMS turbulence cases and is much more constant for the highest turbulence. At a radial distance greater than 30 mm, the ambient turbulence dominates and the velocity is nearly constant and simply equals the ambient turbulence value.

Finally, Fig. 14 shows the important influence of ambient turbulence on spray atomisation through its effect on D_{32} and N. Figure 14 (a) predicts that increasing the ambient turbulence from u'=0 m/s to u'=4 m/s leads to typically a 10% reduction in D_{32} after the end of fuel injection and 15% increase in the number of droplets. Both effects would lead to significantly improved combustion in practical injection systems.

5. Conclusions

It is shown that the turbulence of the gas into which a liquid fuel is injected has a significant influence on the atomisation and evaporation of the latter. Predictions, for which the flow of the ambient gas/fuel vapour mixture is modelled using the popular k-ε turbulence model coupled with the Discrete Phase Model for the liquid fuel phase, are in reasonable agreement with experiments in terms of the overall spray distribution within an injection chamber and its corresponding spray penetration length and widths. Although results using Discrete Phase Models require careful validation and should be used with caution when being used to provide quantitative information, such models are capable of providing detailed information about the nature of the flow field, such as the strength and location of vortices, which have an important influence on fuel mixing and evaporation within an injection chamber.

The results quantify how higher values of ambient turbulence within the gas improve fuel spray atomisation, evaporation and mixing through enhanced momentum exchange between the fuel and ambient gas. This leads to a reduction in the vapour penetration length and the mean diameter of the fuel droplets, together with increases in the spray penetration width and the number of fuel droplets within the spray. The results are of practical relevance to GDI engines since they provide a convenient means of investigating the wetted piston crown problem caused by excessive fuel penetration in the axial direction. Further experimental and computational work into these phenomena is ongoing.

6. Acknowledgement

Ibrahim Elbadawy would like to thank the Egyptian Ministry of Higher Education & Scientific Research (Helwan University) and the University of Leeds for financial support.

References

Agudelo, J., Agudelo, A. and Benjumea, P., Study of Diesel Sprays Using Computational Fluid Dynamics, Revista Facultad de Ingenería Universidad de Antioquia, no. 49, 2009, pp.61-69.

Ashgriz, N., Handbook of Atomization and Sprays-Theory and Applications, Springer, 2011.

Bafekr, S. H., Shams, M., Ebrahimi, R., and Shadaram, A., Numerical Simulation of Pressure-Swirl Spray Dispersion by Using Eulerian-Lagrangian Method, Journal of Dispersion Science and Technology, Volume 32, 2011, pp.47-55.

Banaeizadeh, A., Afshari, A., Schock, H. and Jaberi, F., Large-eddy Simulations of Turbulent Flows in Internal Combustion Engines, Int. J. of Heat and Mass Transfer, Volume 60, 2013, pp.781-796.

Beck, J. C., Watkins, A. P., The Simulation of Fuel Sprays Using the Moments of the Drop Number Size Distribution, Int. J. Engine Res., Volume 5, 2004, pp.1-21.

Boulet, M., Marcos, B., Dostie, M. and Moresoli, C., CFD modeling of heat transfer and flow field in a bakery pilot oven. Journal of Food Engineering, 2010. 97(3): p. 393-402.

Burluka, A. A., El-Dein Hussin, A. M. T. A., Ling, Z. Y. and Sheppard, C. G. W.," Effect of Large-Scale Turbulence on Cyclic Variability in Spark-Ignition Engine, Experimental thermal and Fluid Science J. 43, 2012, pp13-22.

Cooper, D. C. and Yule, A. J., Wave on the Air Core/Liquid Interface of the Pressure Swirl Atomizer, ILASS-Europe, Zurich 2-6 September, 2001.

Delacourt, E., Desmet, B. and Besson, B., Characterisation of Very High Pressure Diesel Sprays Using Digital Imaging Techniques, Fuel, Volume 84, 2005, pp. 859-867.

Desantes, J. M., Margot, X., Pastor, J. M., Chavez, M., and Pinzello, A., CFD-Phenomenological Diesel Spray Analysis Under Evaporative Conditions, Energy and Fuel, Volume 23, 2009, pp. 3919-3929.

Elbadawy, I. M., Gaskell, P. H., Lawes, M., and Thompson, H. M., The Effect of Initial Ambient Turbulence Levels on Iso-octane Injection Sprays, Atomization and Sprays, Volume 21, 2011, pp.799-817.

Faeth, G. M., Hsiang, L. P. and Wu, P. K., Structure and Breakup Properties of Sprays, International of Multiphase Flow, Volume 21, 1995, pp. 99-127.

Fangwei, H., Deming, W., Jiaxing, J., and Xiaolong, Z., Modelling the Influence of Forced Ventilation on the Dispersion of Droplets Ejected from Roadheader-Mounted External Sprayer, Int. J. Mining Science and Technology, Volume 24, 2014, pp.129-135

Gao, J., Jiang, D., Huang, Z., and Wang, X., Experimental and Numerical Study of High-Pressure-Swirl Injector Sprays in a Direct Injection Gasoline Engine, J. Power and Energy, Volume 219, 2005, pp.617-629.

Grover, R. O., Assanis, D. N., Lippert, A. M., ElTahry, S. H., Drake, M. C., Fansler, T. D. and Harrington, D., A Critical Analysis of Splash Criteria for GDI Spray Impingement, 15th Annual Conference on Liquid Atomization and Spray System, Madison, WI., 2002.

Gunnar, L., Turbulence related cyclic variation in combustion, PhD. Thesis, School of Mech. Eng., University of Leeds, 2008.

Jakubik, T., Lawes, M., Woolley, R. and Jicha, M., 2006 , "Study of Ambient Turbulence Effect on Diesel Sprays in a Fan-Stirred vessel", Atomisation and Sprays, Volume 16, pp 687-703.

Jiang, X., Siamas, G.A., Jagus, K., and Karayiannis, T.G., Physical modelling and advanced simulations of gas-liquid two-phase jet flows in atomization and sprays, Progress in Energy and Combustion Science, Volume 36, 2010, pp.131-167.

Kim, K., Kim, D., Jung, Y., and Bae, C., "Spray and Combustion Characteristics of Gasoline and Diesel in a Direct Injection Compression Ignition Engine", Fuel 109, 2013, pp.616-626.

Lim, J., Kim, Y., and Min, K., Characteristics of the Spray and Combustion Process of DME Under Engine Conditions, School of Mechanical and Aerospace Engineering Seoul National University, Korea Seoul, 2004.

Lucchini, T., D'Errico, G., and Ettorre, D., Numerical Investigation of the Spray-Mesh-Turbulence Interactions for High-Pressure, Evaporation Sprays at Engine Conditions, International Journal of Heat and Fluid Flow, Volume 32, 2010, pp. 285-297.

Martínez, S. M., Cruz, F. A. S., Àvila, J. M. R., Muñoz, A. G. and Aceves, S. M., Liquid Penetration Length in Direct Diesel Fuel Injection, Applied Thermal Engineering, Volume 28, 2008, pp.1756-1762.

Nishida, K., Tian, J., Sumoto, Y., Long, W., Sato, K., and Yamakawa, M., An Experimental and Numerical Study on Sprays Injected from Two Hole Nozzles for DISI Engines, Fuel, Volume 88, 2009, pp.1634-1642.

Nwagwe, I. K., Weller,H. G., Tabor, G. R., Gosman, A. D., Lawes, M., Sheppard, C. G. W. and Woolley, R., Measurements and Large Eddy Simulations of Turbulent Premixed Flame Kernel Growth, Proceedings of the Combustion Institute, Volume 28, 2000, pp.59-65.

Oh, H., and Bae, C.," Effects of the Injection Timing on Spray and Combustion Characteristics in a Spray-Guided DISI Engine under Lean-Stratified Operation", Fuel 107, 2013, pp.225-235.

Pastor, J., López, J., Garcia, J., and Pastor, J., A 1D Model for the Description of Mixing-Controlled Inert Diesel Sprays, Fuel, Volume 28, 2008, pp.2871-2885.

Radwan, M. S., Abu El-Yazeed, O. S. M., Elbadawy, I. and Gad, M. M., A Computational Study of In-Cylinder Flow Characteristics in Tow Stroke SIE with Double Intake Manifolds at Different Inclination Angles, 16th International AMME Conference, Cairo-Egypt, 2014.

Rotondi, R. & Bella, G., Gasoline direct injection spray simulation, International Journal of Thermal Sciences, volume 45, 2006, 168-179.

Ryu, J., Kim, H., and Lee, K., A Study on the Spray Structure and Evaporation Characteristic of Common Rail Type Pressure Injector in Homogeneous Charge Compression Ignition Engine, Fuel, Volume 28, 2005, pp.2341-2350.

Saat, A., Fundamental Studies of Combustion of Droplet and Vapour Mixture, Ph.D. Thesis, School of Mech. Eng., Leeds University, UK, 2010.

Schmidt, D. P., Nouar, I., Sececal, P. K., Rutland, C. J., Martin, J. K. and Reitz, R. D., Pressure Swirl Atomization in the Near Field, SAE Technical Paper, 1999-01-0496.

Su, L., Li, X., Zhang, Z., and Liu, F.," Numerical Analysis on the Combustion and Emission Characteristics of Forced Swirl Combustion System for DI Diesel Engines, Energy Conversion and Management 86, 2014, pp.20-27.

Sulaiman, S. A., Burning Rates and Instabilities in the Combustion of Droplet and Vapour Mixtures, Ph.D. Thesis, School of Mech. Eng., Leeds University, UK, 2006.

Takagi, Y., A New Era in Spark Ignition Engines Featuring High Pressure Direct Injection, Twenty-Seventh Symposium (International) on Combustion/The Combustion Institute, 1998, pp.2055-2068.

Takeuchi, S., and Douhara, N., Effect of Turbulence Characteristic in the Spray Combustion, JSME International Journal, Volume 48, 2005, pp.151-155.

Takeuchi, S., and Douhara, N., Influences of Turbulence Characteristic on the Dispersion Behavior of Droplets in the Spray Flame, Journal of Thermal Science and Technology, Volume 3, 2008, pp.266-277.

Tomar, G., Fuster, D., Zaleski, S., Popinet, S., Multiscale Simulation of Primary Atomization, International Journal of Computers & Fluids, Volume 39, 2010, pp.1864-1874.

Turkcan, A., Ozsezen, A. N., and Canakci, M." Experimental Investigation of the Effects of Different Injection Parameters on a Direct Injection HCCI Engine Fueled with Alcohol–Gasoline Fuel Blends", Fuel Processing Technology 126, 2014, pp.487-496.

Wei, S., Ji, K., Leng, X., Wang, F., and Liu, X.," Numerical Simulation on Effects of Spray Angle in a Swirl Chamber Combustion System of DI (Direct Injection) Diesel Engines", Energy, 2014,pp.1-6.

Wright, Y. M., Numerical Investigation of Turbulent Spray Combustion with Conditional Moment Closure, PhD Thesis, Swiss Federal Institute of Technology Zurich, 2005.

Zhao, F., Lai, M. C. and Harrington, D. L., Automotive Spark-Ignited Direct-Injection Gasoline Engines, Progress in Energy and Combustion Science, Volume 25, 1999, pp.437-562.

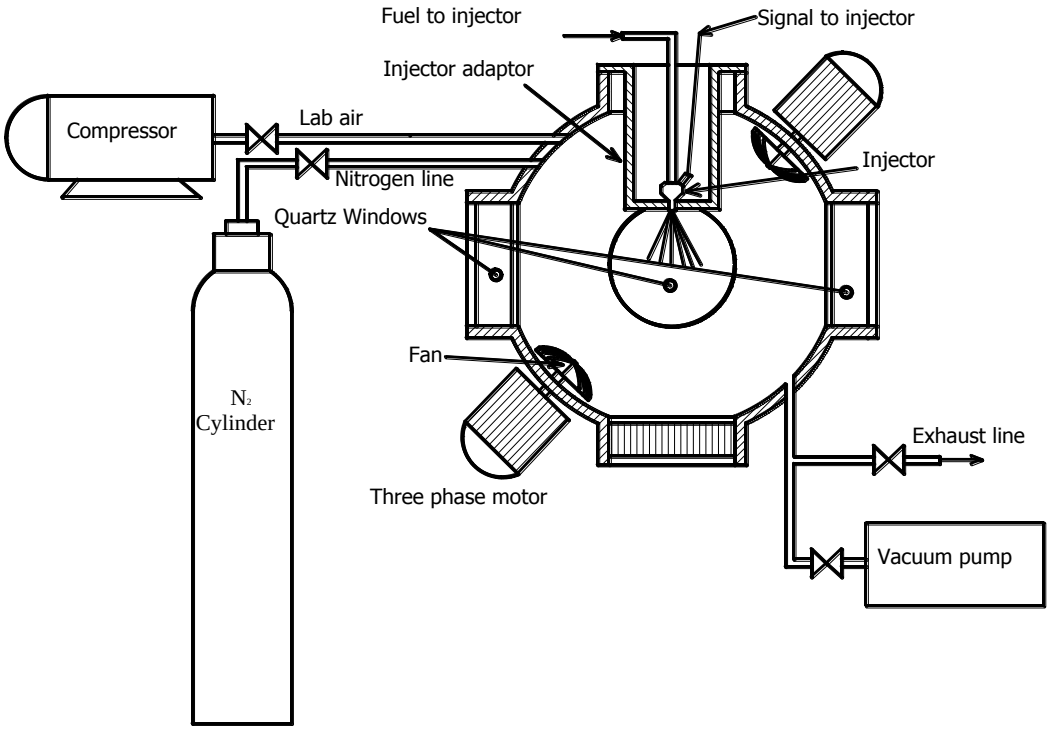

Fig. 1(a) Schematic of MKII vessel system.

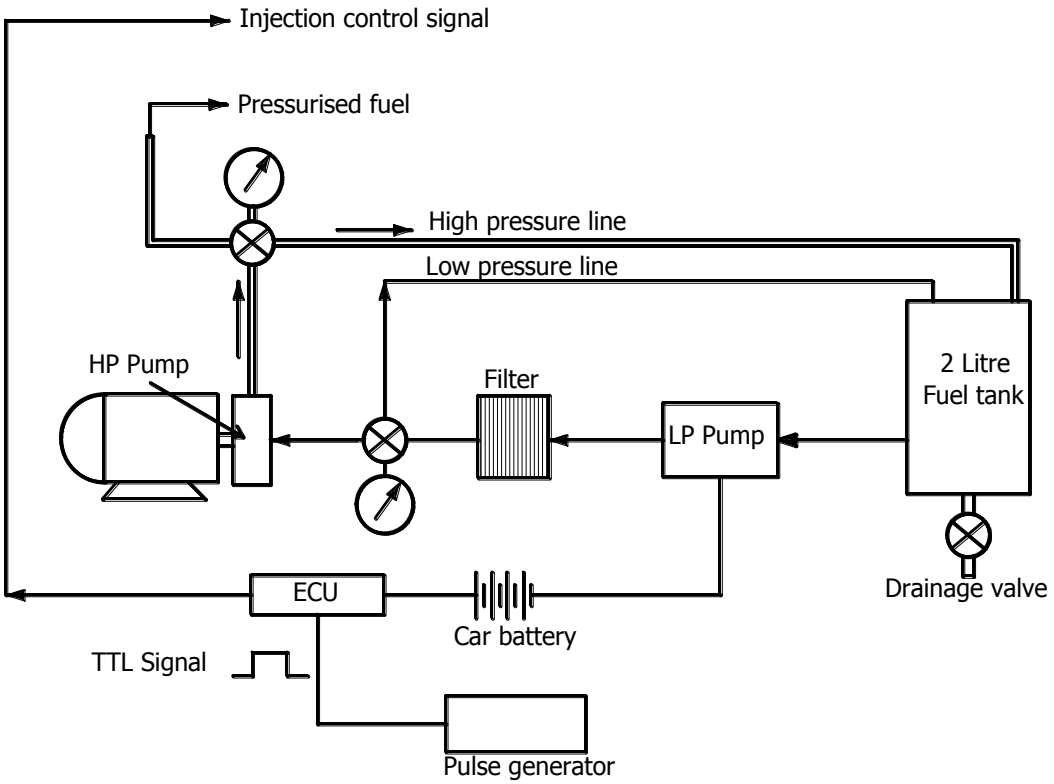

Fig. 1(b) Schematic of the experimental fuel injection system.

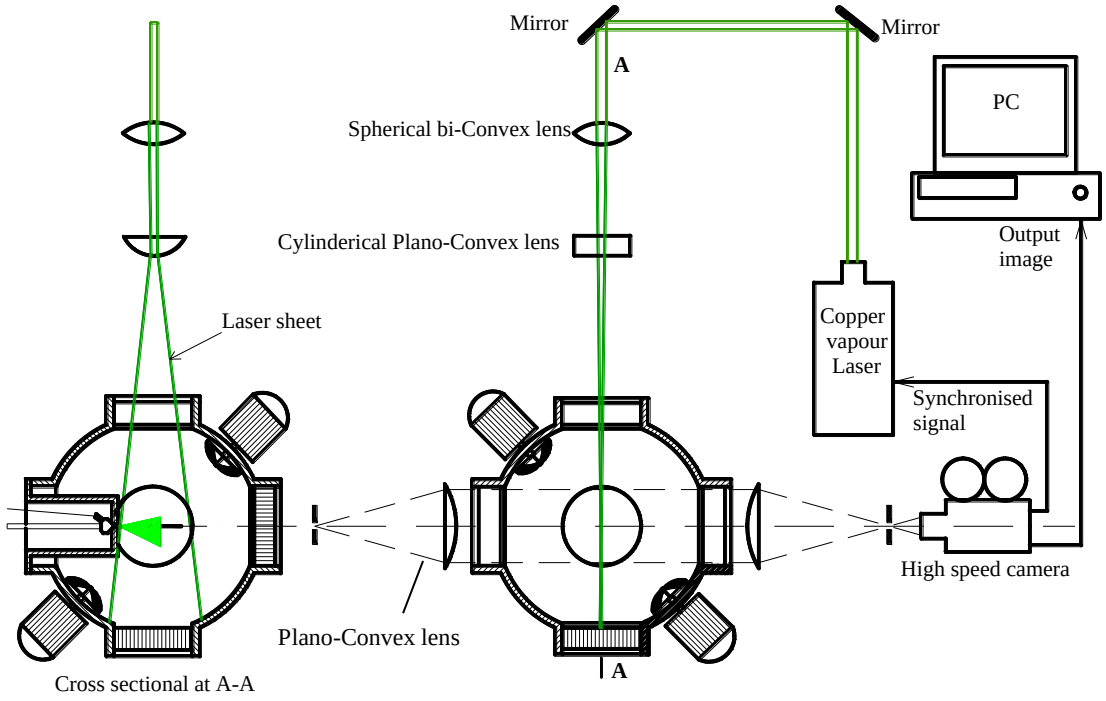

Fig. 1(c) Schematic of Mie scattering laser sheet and Schlieren techniques.

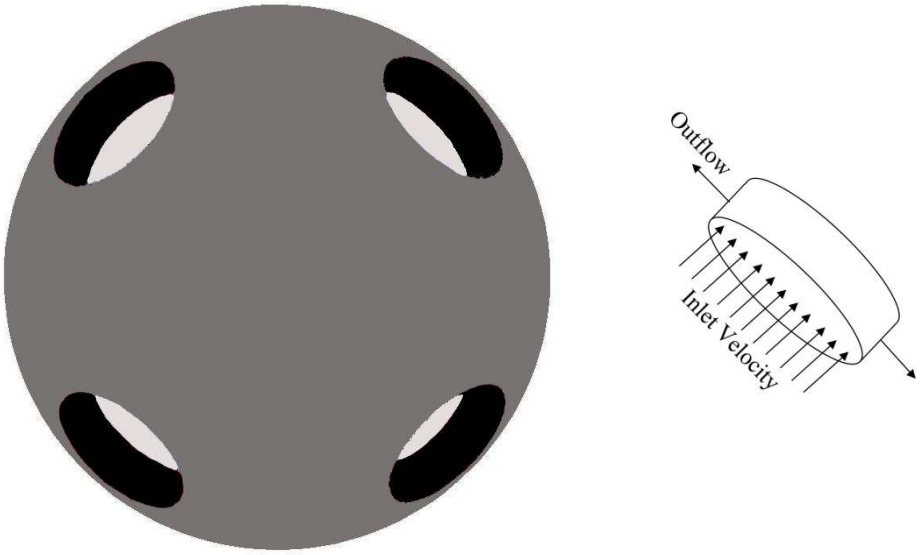

(a)

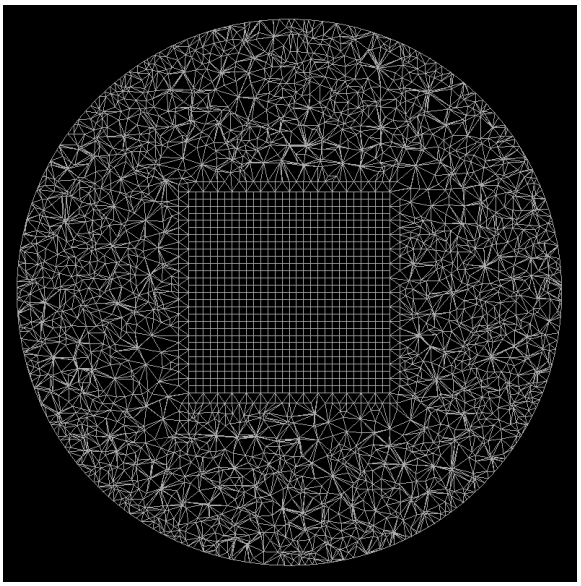

(b)

Fig. 2 Flow domain used in the CFD analyses: (a) main cylindrical geometry (left) with an expanded view of an inflow/outflow cylinder (right); (b) fine mesh used in the central fuel injection system.

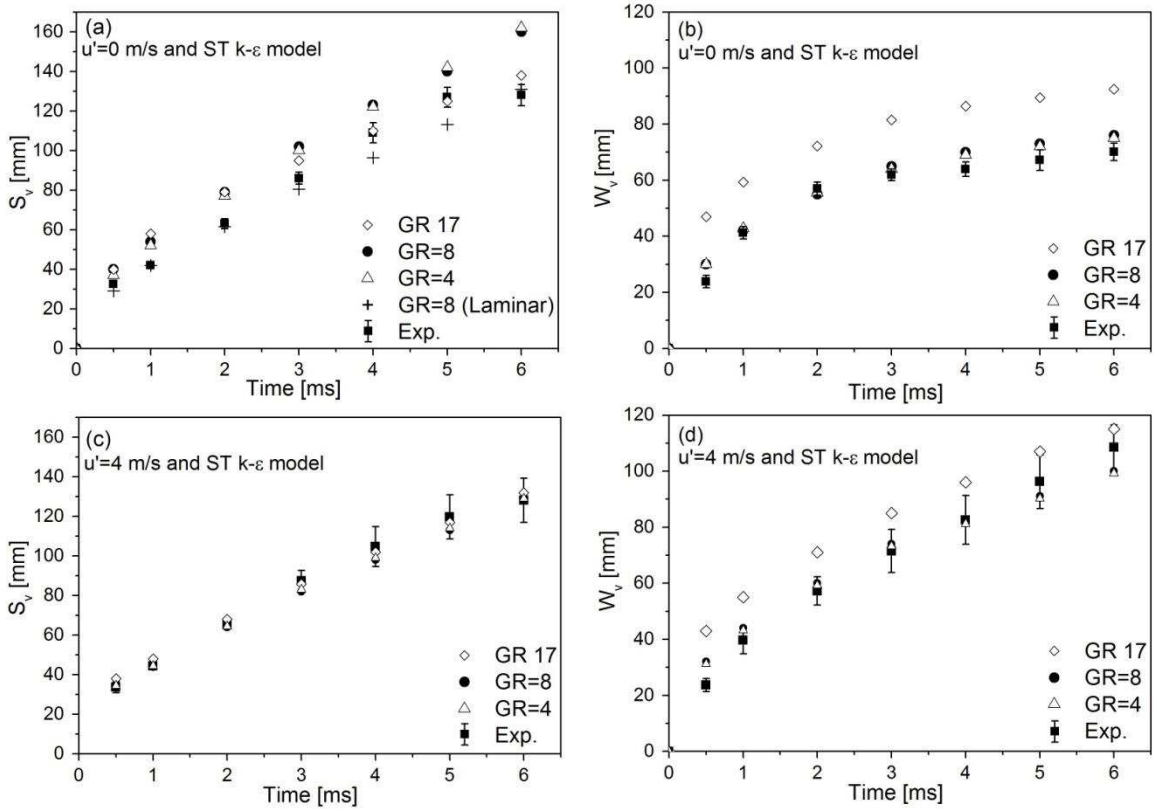

Fig. 3 Effect of mesh density on measured and predicted (a, c) S_V, and (b, d) W_V, for injection into quiescent ambient nitrogen with u'=0 m/s and turbulent condition with u'=4 m/s. Experimental uncertainties are specified by the error bars, Elbadawy et al. (2011).

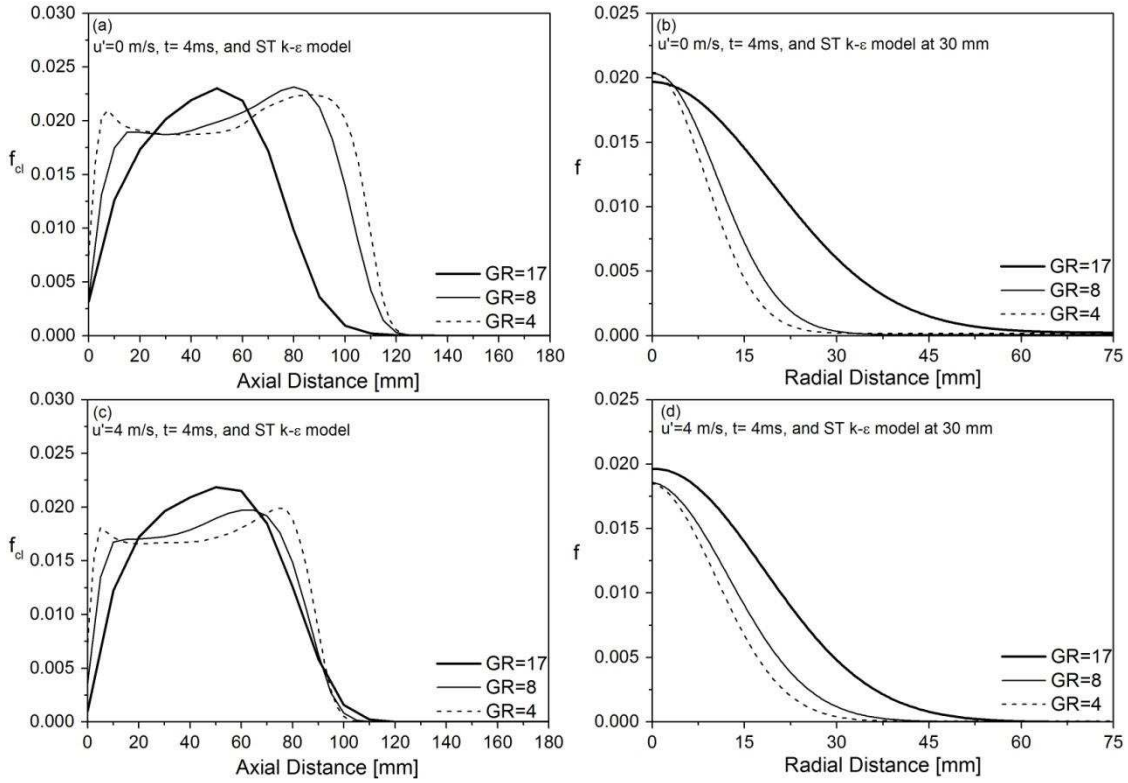

Fig. 4 Effect of mesh density on fuel vapour mass fraction for injection into quiescent ambient nitrogen with u'=0 m/s and u'=4 m/s at t=4ms: (a, c) f_{cl} and (b, d) f at 30mm from the injector axis.

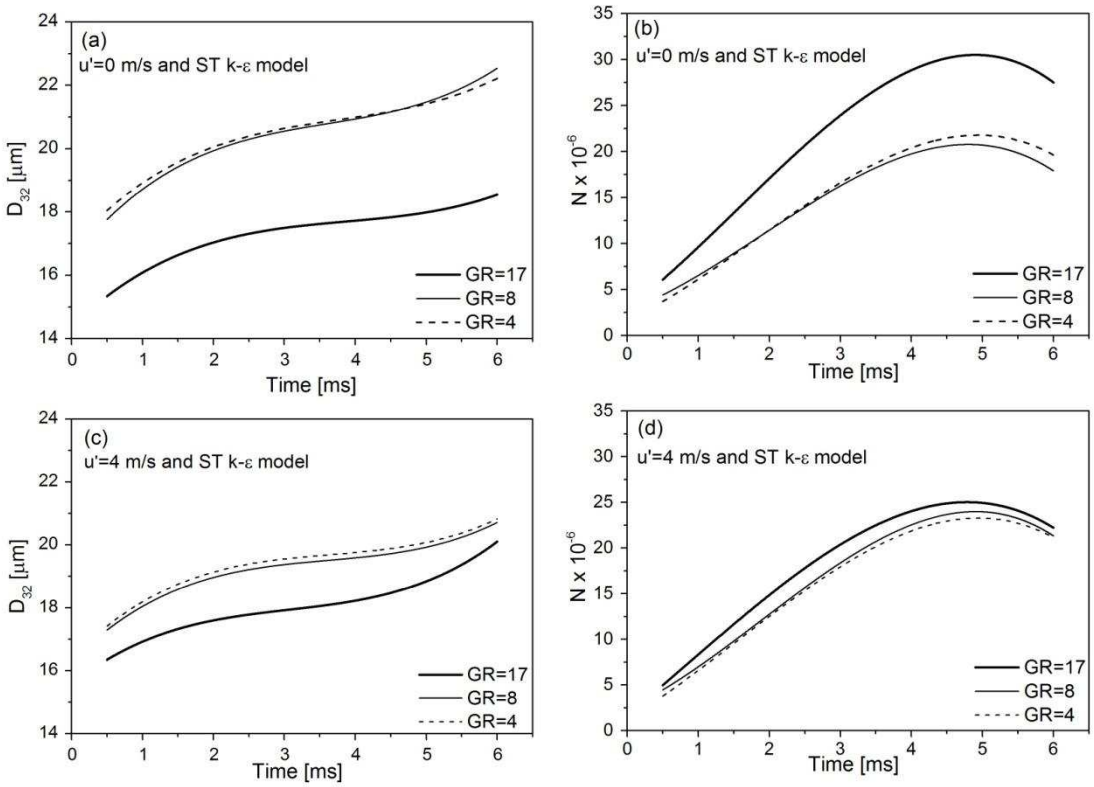

Fig. 5 Effect of mesh density on (a, c) D_{32} and (b, d) N as a function of time at u'=0 and 4 m/s, using the standard k-ε model.

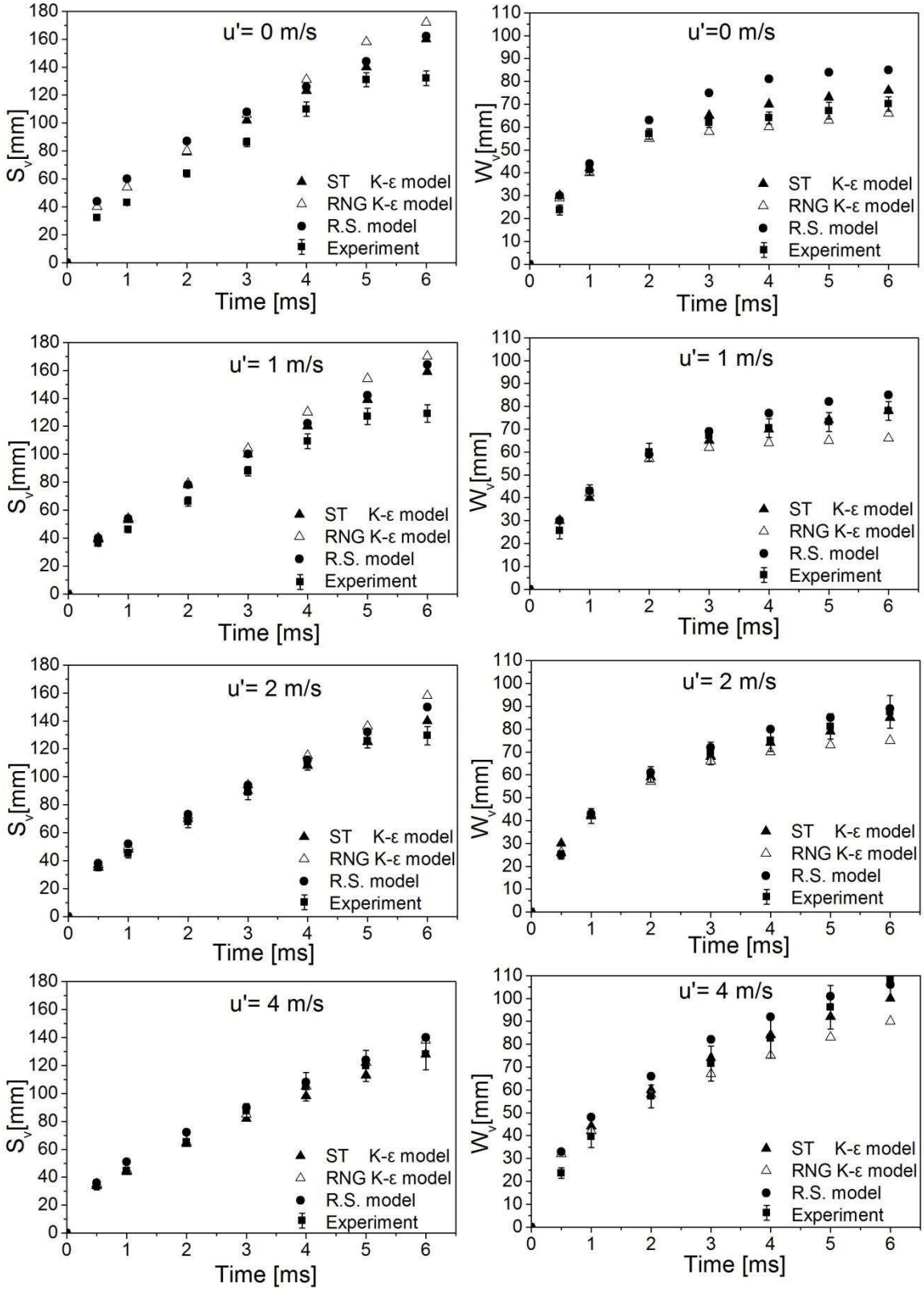

Fig. 6 The effect of different RANS turbulence models with GR=8 on the predictions of: (a) S_V, and (b) W_V, for injection into ambient nitrogen with u'=0, 1, 2 and 4m/s. Experimental uncertainties are specified by the error bars, Elbadawy et al. (2011).

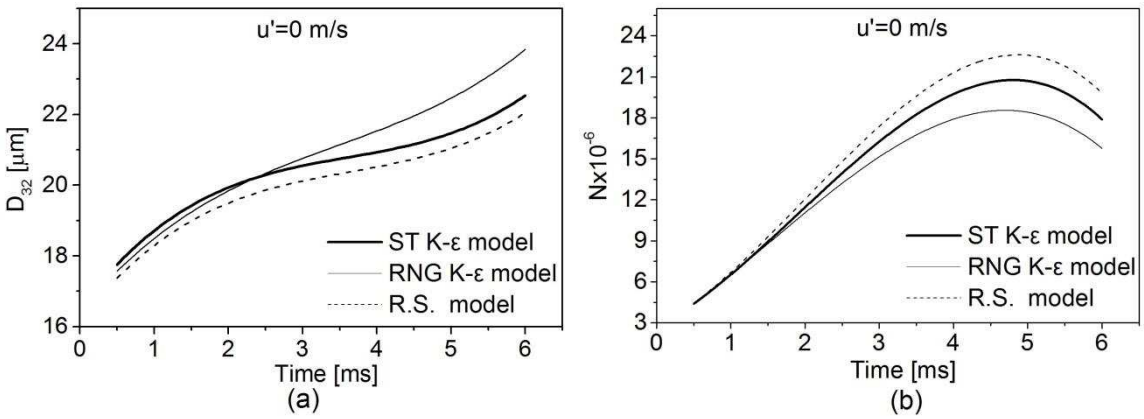

Fig. 7 The effect of different RANS turbulence models on (a) D_{32} and (b) N as a function of time, for injection into quiescent ambient nitrogen with u'=0 m/s.

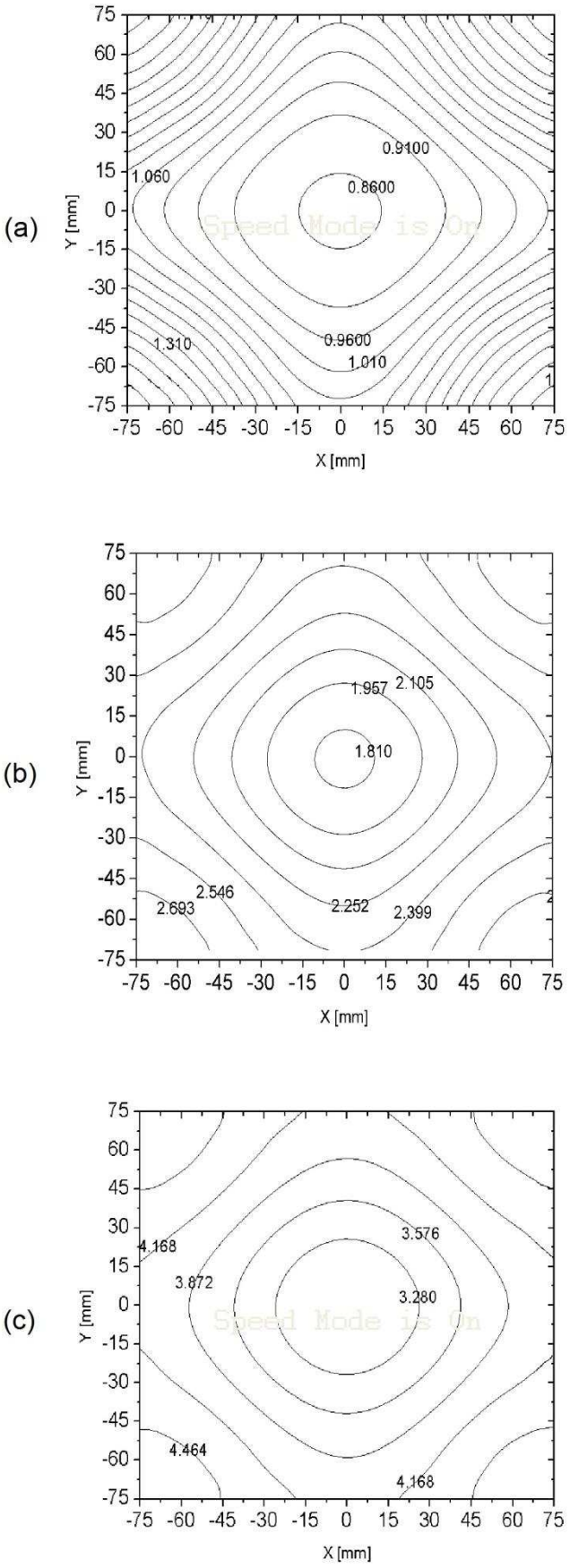

Fig. 8 Local RMS turbulence velocity contours, using a standard k-ε turbulence model, for (a) ù=1m/s, (b) ù=2 m/s and (c) ù=4 m/s.

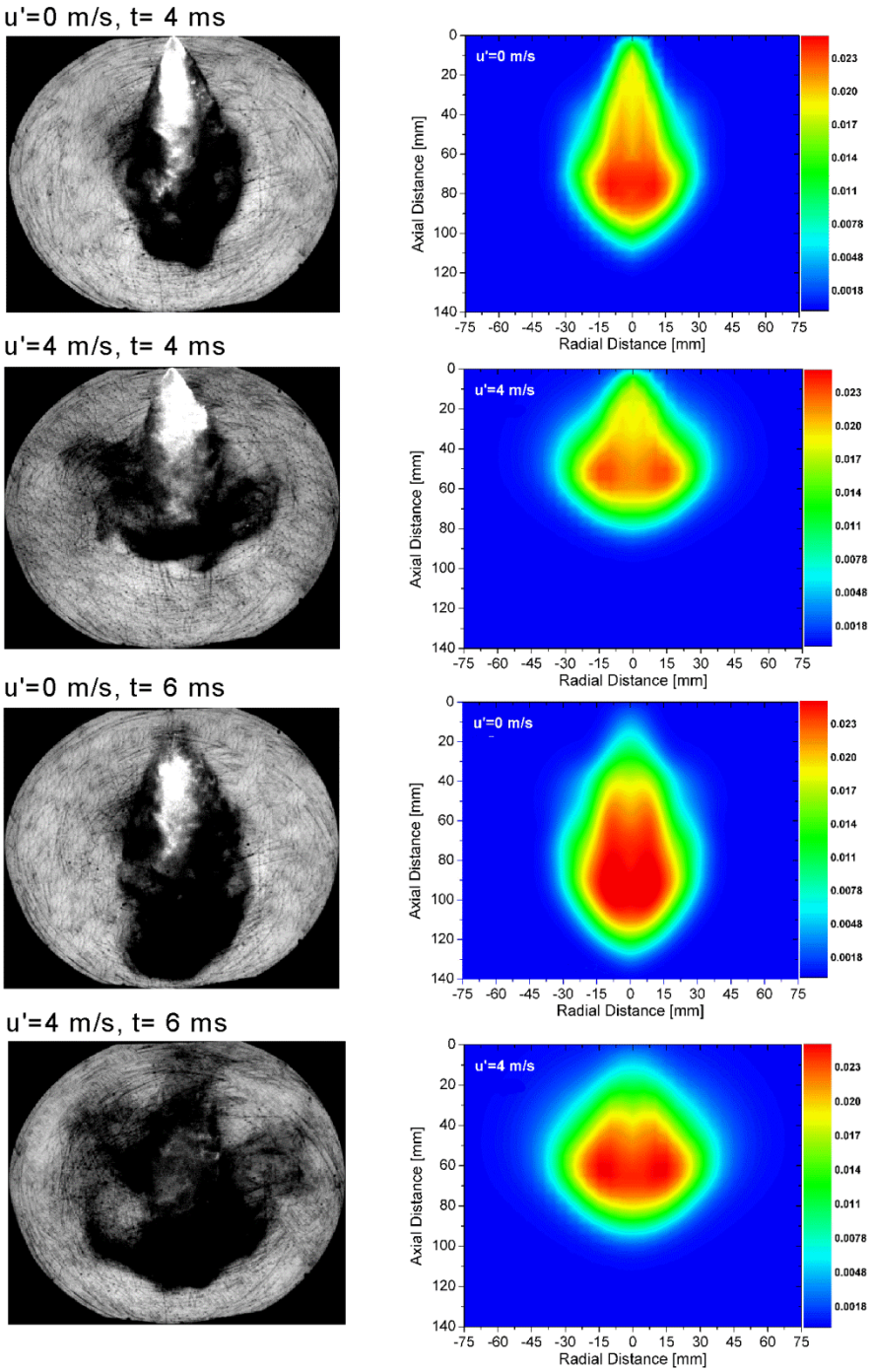

Fig. 9 Comparison of experimental (left) and computational predictions (right) of fuel evaporation under laminar (ù=0 m/s) and turbulent conditions (ù=4 m/s) at t=4ms and 6ms.

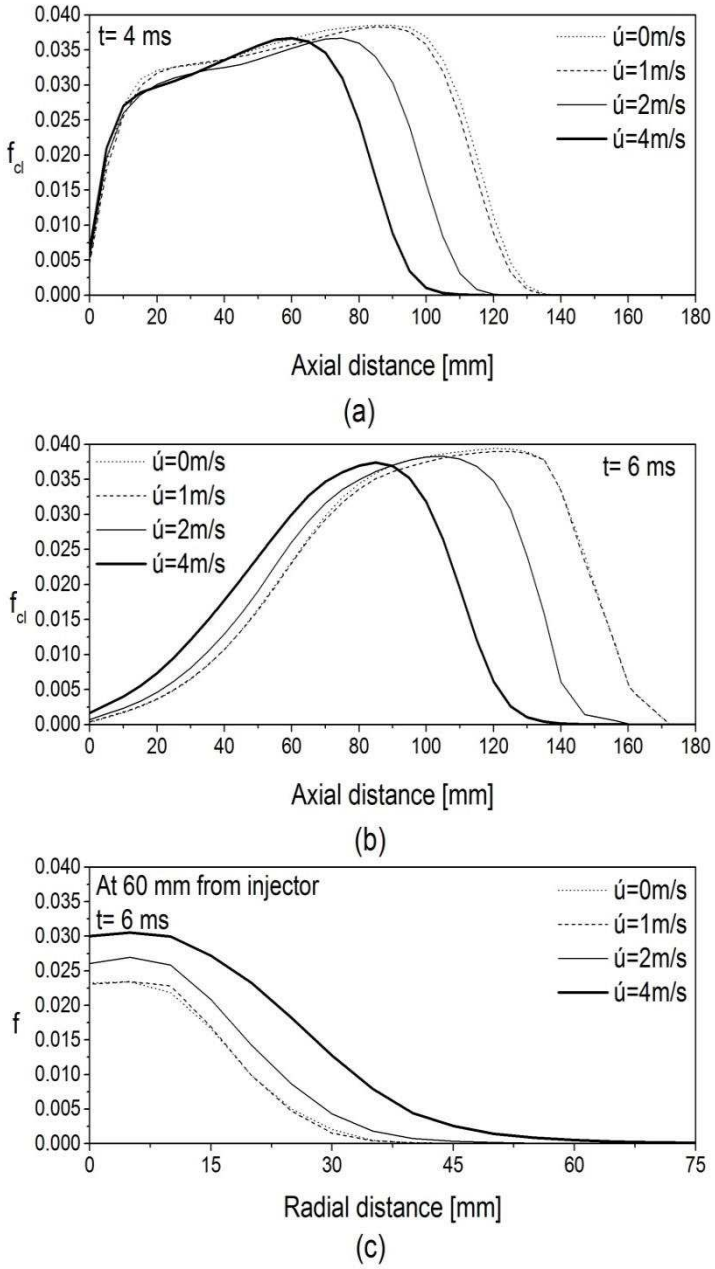

Fig. 10 The effect of ambient turbulence on predicted f_{cl} at (a) t=4ms and (b) t=6ms; and predicted f at (c) 60mm from the injector and t=6ms.

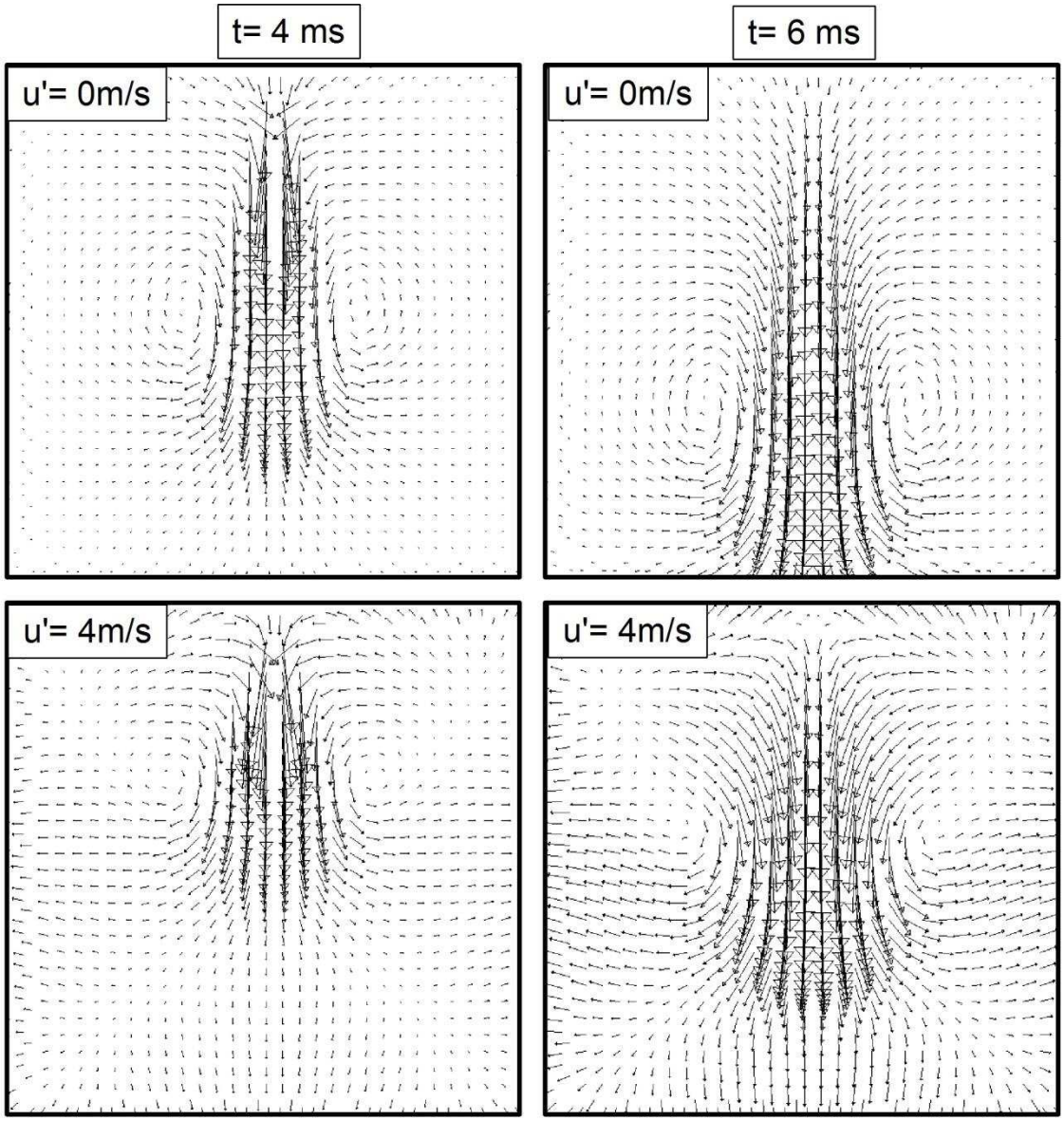

Fig. 11 Comparison between predicted gas velocity vectors for u’=0 and u’=4m/s at t=4 and 6ms.

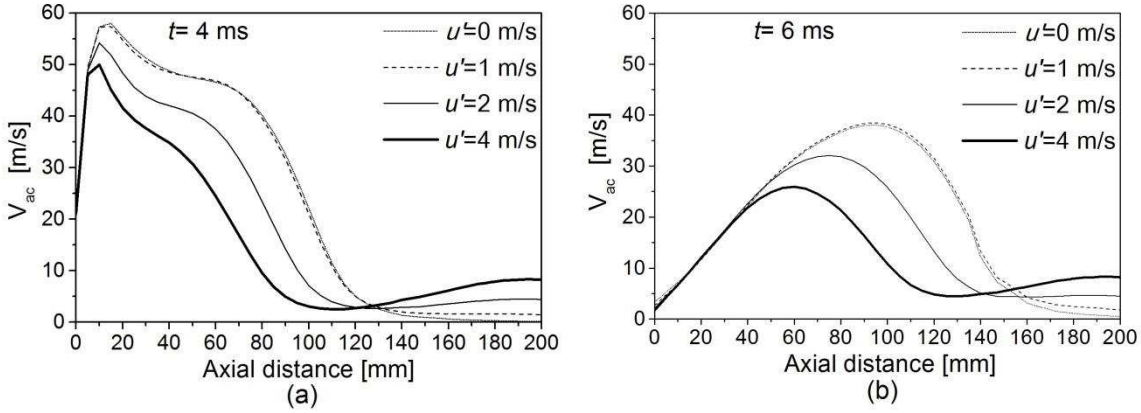

Fig. 12 Effect of ambient turbulence on V_{ac} along the injector axis at (a) t=4 ms and (b) t=6 ms

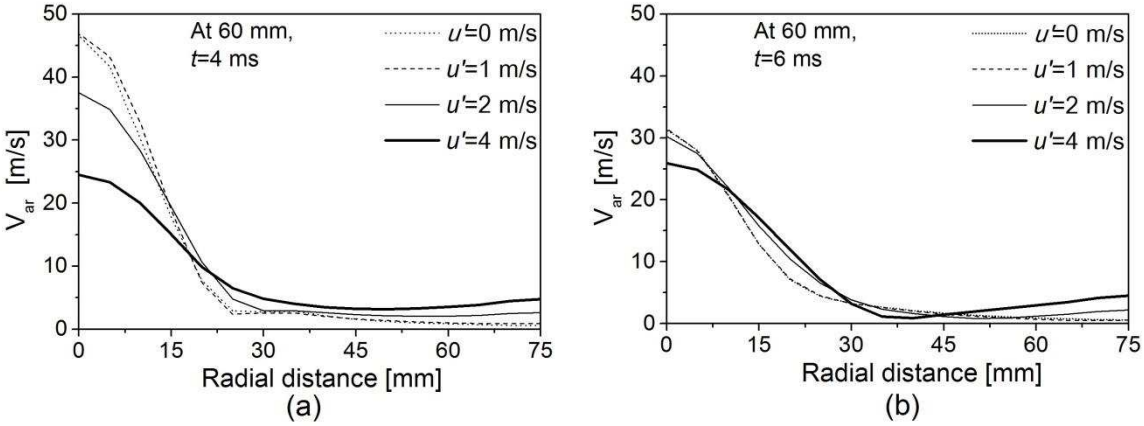

Fig. 13 Effect of ambient turbulence on V_{ar} at a distance of 60 mm from the injector at (a) t=4 ms and (b) t=6 ms

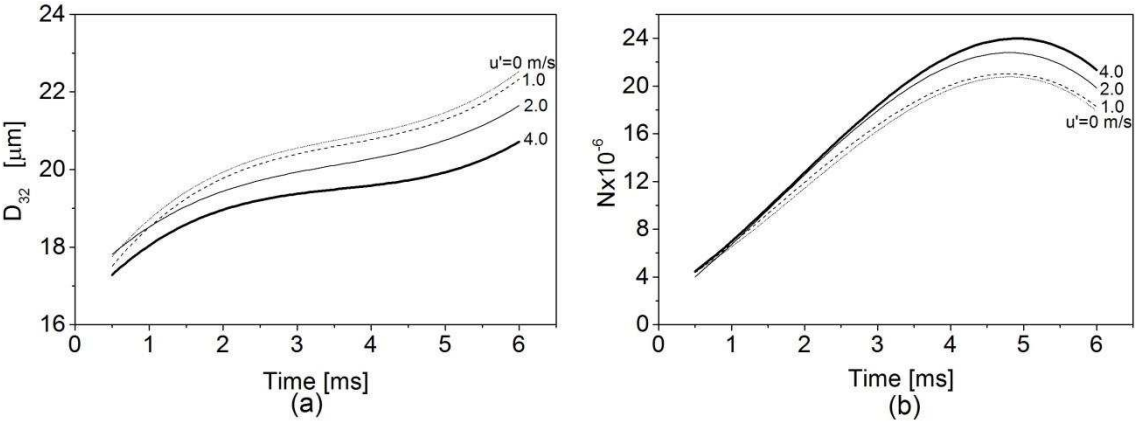

Fig. 14 Effect of ambient turbulence on predicted (a) D_{32} and (b) N.